Catena 212 (2022) 106100

Contents lists available at ScienceDirect

Catena

journal homepage: www.elsevier.com/locate/catena

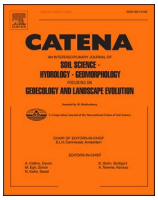

Combining FDR and ERT for monitoring soil moisture and temperature patterns in undulating terrain in south-eastern Norway

Dominika Krzeminska *, Esther Bloem, Torsten Starkloff [1], Jannes Stolte

Norwegian Institute of Bioeconomy Research (NIBIO), Division of Environment and Natural Resources, P.O. Box 115, 1431 Ås, Norway

ARTICLE INFO

Keywords:
Soil moisture
Local terrain heterogeneities
Slope aspects
ERT
Soil erosion

ABSTRACT

The occurrence of freeze–thaw cycles modifies water infiltration processes and surface runoff generation. Related processes are complex and are not yet fully investigated at field scale. While local weather conditions and soil management practices are the most important factors in both runoff generation and surface erosion processes, local terrain heterogeneities may significantly influence soil erosion processes in catchments with undulating terrain.

This paper presents a field-based investigation of spatial and temporal heterogeneities in subsurface soil moisture and soil temperature associated with freezing, thawing, and snowmelt infiltration. The field setup consists of a combination of traditional point measurements performed with frequency domain reflectometry (FDR) and electrical resistivity tomography (ERT). The transect was approximately 70 m long and spanned an entire depression with a north-facing slope (average slope of 11.5%) and a south-facing slope (average slope of 9.7%). The whole depression was entirely covered with stubble.

Observed resistivity patterns correspond well to the measured soil moisture patterns. During the observation period, the north facing slope froze earlier and deeper compared with the south facing slope. Freeze–thaw cycles were less pronounced in the north-facing slope than in the south-facing slope. There were also differences in soil temperature and soil moisture patterns between lower and upper parts of the monitored depression. These indicate that initiation and development of runoff related processes, and consequently soil erosion, in regions with freeze–thaw cycles may differ significantly depending on local terrain characteristics. Consequently, it indicates that spatial terrain heterogeneities, especially slope aspects, may be important when studying soil erosion processes, water flow and nutrient leaching in lowlands where patchy snowpacks and dynamic freeze–thaw cycles are predominating.

1. Introduction

In most climates, soil erosion is governed by the surface runoff of water during excessive rainfalls and/or snow melting. Soil erosion is one of the most serious threats to productive agricultural land (Weigert and Schmidt, 2005; Boardman et al., 2009; Yakutina et al., 2015). This is especially true in Norway, where the amount of cultivated land is limited and often only has a thin layer of nutrient rich soil (Lundekvam et al., 2003). Under Nordic climate conditions soil erosion rates in winter and early spring account for a major part of annual soil, phosphorus, and nitrogen losses in agricultural catchments (Deelstra et al., 2011). Snowmelt, combined with rain and frozen (sub-)soil, may lead to severe runoff and consequent soil erosion (Lundekvam and Skøien, 1998; Øygarden, 2003; Deelstra et al., 2009). However, the severity of the erosion is often amplified by preceding winter conditions. The occurrence of freeze–thaw cycles modifies water infiltration processes, surface runoff generation (Iwata et al., 2011, Ban et al., 2016) and erosivity of the soil material (Ollesch et al., 2006). The processes associated with freeze–thaw cycles are complex and their implications for water flow in (partially) frozen soil are still not fully understood (Ireson et al., 2013). Moreover, despite increasing research attention, the amount of relevant field observations at catchment scale is still limited (e.g., Øygarden, 2003; He et al., 2015; Starkloff et al, 2017; Holten et al., 2018).

The three main soil-related factors that determine the speed of snowmelt and/or rain infiltration into (partly)frozen soil, and thus the

* Corresponding author.
E-mail address: dominika.krzeminska@nibio.no (D. Krzeminska).
[1] Present workplace: The Norwegian Water Resources and Energy Directorate (NVE), NO - 3103 Tønsberg, Norway.

https://doi.org/10.1016/j.catena.2022.106100
Received 21 July 2021; Received in revised form 28 January 2022; Accepted 30 January 2022
Available online 21 February 2022

extent of surface runoff and erosion, are: 1) initial water content (before freezing), 2) frost depth and 3) soil temperature at the time of snowmelt/rainfall (Al-Houri et al., 2009; Watanabe et al., 2013). Monitoring these properties at catchment scale is complicated by the need to account for spatial heterogeneity. Research has shown that runoff and soil erosion can vary greatly depending on slope characteristics such as slope angle, length and aspect (Shanley and Chalmers, 1999; Laker, 2004). This indicates the importance of taking into account local therein heterogeneities, especially slope aspect, when studying soil erosion processes in lowland agricultural catchments with undulating landscape. To increase understanding of processes that influence snowmelt infiltration and runoff in such catchments, field-based observation of subsurface processes during freezing, thawing and snowmelt, ideally accounting for local terrain heterogeneities (i.e., slope, aspect, gullies) is needed.

Soil temperature and soil moisture monitoring are commonly used surveying techniques in studies on hydrogeological processes (Tabbagh et al., 1999; Cheviron et al., 2005) and especially on percolation rates in the vadose zone (Constantz et al., 2003). However, these methods provide commonly only point measurements. In order to focus on the spatial heterogeneity effects, non-invasive geophysical techniques are considered effective monitoring methods at field scale (Hubbard and Rubin, 2000; Vereecken et al., 2006; Binley, 2015). Electrical resistivity tomography (ERT) presents an alternative approach to monitoring subsurface hydrological conditions and processes across a range of materials and spatial scales (e.g., French et al., 2002; French and Binley, 2004; Jayawickreme et al., 2008; Alamry et al., 2017). The resistivity of the subsurface reflects a combination of soil texture, water/fluid saturation and pore fluid properties, such as salinity (e.g., Depountis et al., 2001). In permafrost research, ERT methods have been widely used to estimate the unfrozen water content based on significant contrasts in electrical resistivity between frozen and unfrozen soil (French et al., 2002, Krautblatter and Hauck, 2007, Fortier et al., 2008, Dafflon et al., 2013). Two-dimensional time-lapse ERT, in which ERT measurements are repeated over time, can give a rapid, qualitative overview of the evolution of soil moisture and/or ice content over large areas, assuming that soil physical properties are constant over time (French et al. 2002; French and Binley, 2004; Cassiani et al., 2006; Kemna et al., 2006; Scherler et al., 2010).

To investigate the potential of the field-based monitoring techniques to capture the dynamics of soil temperature and soil moistures patterns, depending on terrain heterogeneity, during winter conditions, we combined point measurements (soil temperature and soil moisture) with spatially distributed geophysical monitoring (ERT). This paper presents the results of these observations, with the focus on local terrain heterogeneities and their influence on freezing and thawing patterns in the soil.

2. Case study description

The study area is the Skuterud agricultural catchment, located in south-eastern Norway (Fig. 1). The field investigations were carried out in the Gryteland catchment (0.29 km^2) characterised by undulating landscape (elevation: 106–141 m, slope 2–10%) covered by approximately 60% arable land and 40% coniferous forest. The soil types of the arable land can be divided into two groups: 1) levelled clay loam (Stagnosol) and silty clay loam (Albeluvisol) and 2) sandy silt on clay (Umbrisol) and sand to loamy medium sand (Histic Gleysol). The two soil groups are not always clearly distinguishable in the field (Solbakken, 2015). A subsurface drainage system was installed in the arable land in the 1960s, leading to an unsaturated zone of approximately 1 m depth.

The mean annual temperature is 5.3 °C and the mean annual precipitation is 785 mm (Thue-Hansen and Grimenes, 2014). The winter weather conditions are usually relatively unstable, with alternating periods of freezing and thawing and several snowmelt events (Kværnø and Øygarden, 2006). The register of snow conditions is available via

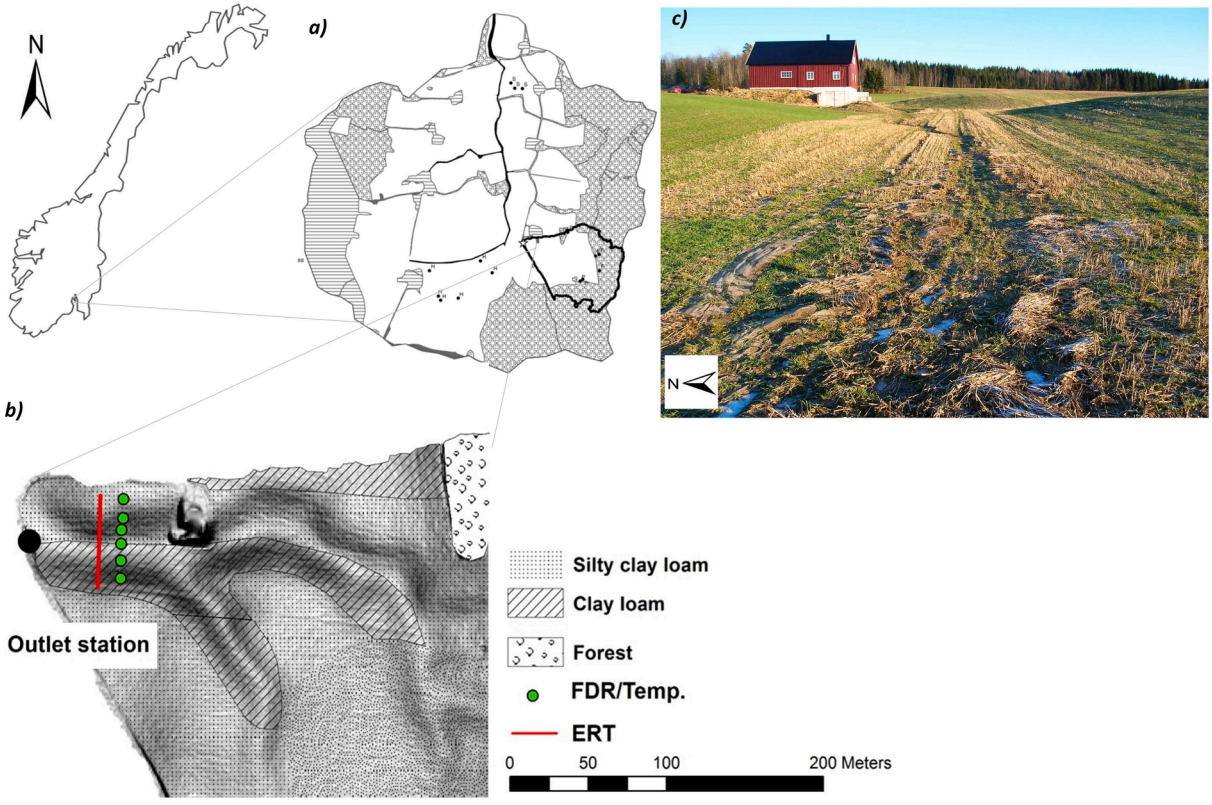

Fig. 1. (a) Location of the Gryteland catchment (outlined in black) within the Skuterud catchment in Norway; (b) location of experimental transect and monitoring equipment within the Gryteland catchment; (c) a view on the Gryteland catchment (photo: J. Stolte).

Varsom Xgeo (http://www.xgeo.no/), an expert tool used for preparedness, monitoring, and forecasting of floods, landslides and avalanches in Norway. In addition, manual meaurements of snow depth was performed during three field visits.

3. Methodology

3.1. Experimental site set up

The experimental transect was established in the Gryteland catchment (Fig. 1 a, b). The soil along the transect is clay loam and silty clay loam with 13% sand, 58% silt and 29% clay. In the period 2014–2016, oats were grown in the entire area of Gryteland. There was no tillage after harvest in 2013, leaving the fields covered in stubble. In 2015 after harvest, secondary tillage was done on the slopes using a cultivator, leaving the dry waterways covered with stubble. The experimental transect is located in the area covered with stubble (Fig. 2).

The transect was 71 m long and covered a depression with a north-facing slope (with an average slope of 11.5%) and a south-facing slope (with an average slope of 9.7%) (Fig. 1b). The following sections along the experimental transect were defined: south-facing top (SFT) with 8.3% slope, south-facing middle (SFM) with 14% slope, south-facing bottom (SFB) with 6.5% slope, north-facing bottom (NFB) with 8% slope, north-facing middle (NFM) with 16% slope and north-facing top (NFT) with 8% slope.

3.2. Soil temperature and soil moisture measurements

Six nests, each with five Decagon 5 TM temperature and frequency domain reflectometry (FDR) sensors were installed along the transect (Fig. 1b). Soil water content (θ_{liquid} [$m^3.m^{-3}$]) and soil temperature (T_{soil} [^oC]) readings were automatically recorded every 30 min at five depths: 0.05, 0.10, 0.20, 0.30 and 0.40 m. It should be noted that the soil water content, calculated from the dielectric permittivity of the soil matrix and measured using the FDR probes, represents only the liquid soil water content, not water in the form of ice. However, the drop in θ_{liquid} when T_{soil} moves below 0 °C is a good indication that soil water in the soil profile is starting to freeze and ice is beginning to form (Starkloff et al., 2017).

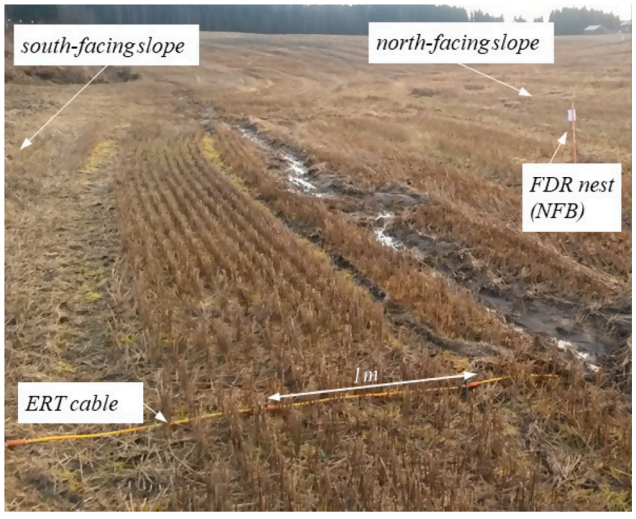

Fig. 2. View of the depression where the experimental transect was located. Photo taken in December 2015, during equipment installation. FDR stands for frequency domain reflectometry sensors nest and NFB stand for north-facing bottom section of the transect. The spacing between the electrodes along ERT cable is 1 m and it serves as scale indicator. (Photo: D. Krzeminska).

3.3. Electrical resistivity tomography (ERT) measurements

3.3.1. Field data collection

The purpose of the ERT survey is to determine the subsurface resistivity distribution by performing measurements at the earth's surface. With ERT, an electrical current (I [A]) is induced in the ground using two current electrodes. The resulting voltage difference (U [V]) is measured by two potential electrodes (Fig. 3; Nijland et al., 2010; Binley, 2015). From the current, the voltage difference and the geometrical factor (which depends on the arrangement of the electrodes), the apparent resistivity (R) of the ground can be derived. The apparent resistivity is an average value for the ground taken as a homogeneous half-space. Increasing the spacing between the electrodes provides more information about the deeper part of the subsurface. A 2D distribution of apparent electrical resistivities along a transect can be obtained by combining many different combinations of 'single' measurements. The apparent resistivity values obtained are processed and, finally, a resistivity model is created.

In our study, the ERT transect was 71 m long, with 1 m spacing between the electrodes (total 72 electrodes). The electrodes remained in the soil during the whole experimental period to guarantee that measurements were made at the same locations every time and to ensure a best possible quality of the readings (Michot et al., 2003).

ERT measurements were performed by a Syscal Pro Switch (Iris instrument) with a conventional Wenner electrode configuration as for its optimal characteristics regarding depth of investigation, ability to resolve vertical changes, and signal-to-noise ratio (Loke, 2000). Normal and reciprocal data (swapping the potential and current electrodes) were collected directly one after another, using a 100 ms current injection. The ERT readings were collected one time per week and, if needed, after a sudden change in weather conditions. In total, 11 ERT series were recorded.

3.3.2. Data processing

First, reciprocal measurements were used to identify and remove outliers (measurements with an error between the normal and reciprocal greater than 10%) prior to data inversion. Thereafter, raw ERT data were processed using R2 software (v2.7a; Binley, 2013) in inverse mode (Binley and Kemna, 2005).

We used a quadrilateral grid for finite element modelling, with horizontal boundaries between −1024 m and 1095 m (while the electrodes were located from 0 m to 71 m) and vertical boundaries between

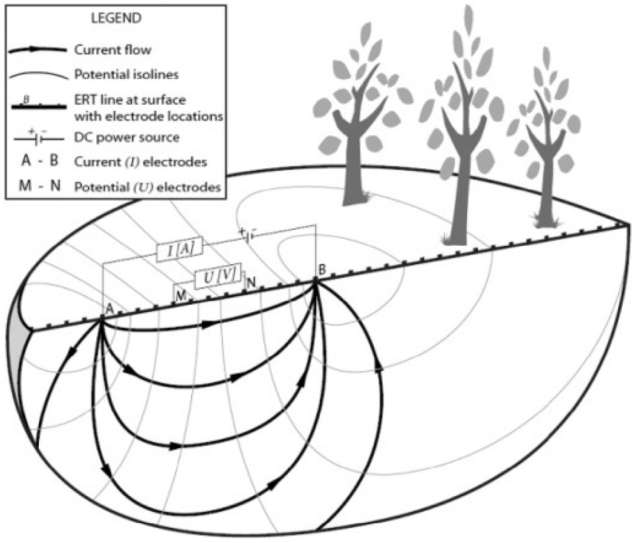

Fig. 3. Schematic diagram of resistivity measurement in a uniform medium (after Nijland et al., 2010).

0 m and −109.9 m from the surface (while we are interested in the top meters only). Using this 'larger' grid allowed the assumption that the inversion results in the area of interest were realistic for an infinite half-space. For the area of interest, the grid resulted in a spatial resolution of 0.5 m horizontally and 0.1 m vertically.

The inverse solution was based on a regularised objective function combined with weighted least squares (an 'Occams' type solution) as defined in Binley and Kemna (2005). For the inversion we used a standard error distribution with an offset error (a_wgt) equal to 0.001 and a relative error (b_wgt) equal to 0.02.

All the collected ERT datasets converted in three to seven iterations with an average root-mean-square error of 1.01 relative to measured noise, calculated by the stacking error. For each of the 11 datasets collected, we obtained the horizontal and vertical distribution of the physical resistivity property.

4. Results

4.1. Soil temperature and soil moisture measurements

Fig. 4a shows the weather data: air temperature (T_{air}) and precipitation (P) and Fig. 4b shows the soil temperature (T_{soil}) at the five depths (0,05, 0,10, 0.20, 0.30 and 0.40 m), along the experimental transect.

From the T_{soil} measurements it is easy to distinguish between freezing and thawing periods and to identify the snowmelt period at the end of the winter season. At the beginning of the monitoring period (December 2015), when T_{air} was still above 0 °C and there was no snow cover, T_{soil} tracked T_{air}. As snow cover developed (starting January 2016), the daily

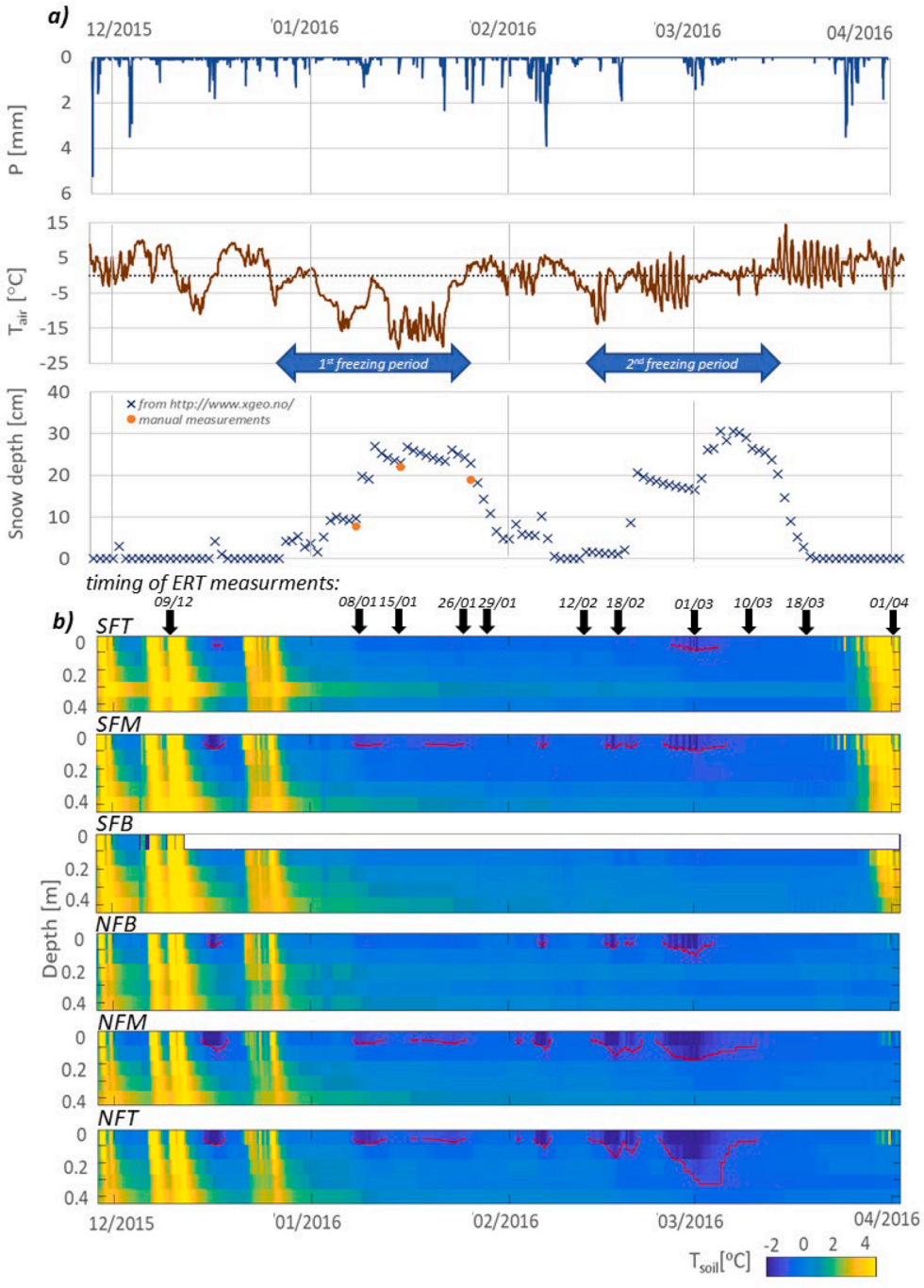

Fig. 4. Monitored data: (a) precipitation (P), air temperature (T_{air}) and snow depth. The Black dotted line at T_{air} figure denotes the 0 °C line; (b) vertical profiles (0.05, 0.10, 0.20, 0.30, 0.40 m depth) of soil temperature (T_{soil}) at six locations along the experimental transect (SFT, SFM, SFB, NFB, NFM, NFT). The black arrows indicate the dates when ERT measurements were performed. The red lines denote soil with $T_{soil} < 0$ °C. The white area within SFB section denotes a period with no measurements due to technical problems.

T_{soil} amplitude gradually reduced, as did the temperature differences in the soil profile. During two freezing periods with snow cover of 20–30 cm depth (25/12/2015 – 26/01/2016 and 11/02/2016–13/03/2016), the isolation effect of snow cover was clear: in general, daily temperature variations of T_{soil} were not visible and T_{soil} did not follow the drop in T_{air} (below −15 °C). However, the freeze and thaw periods in the soil were clearly visible. During the first freezing period (25/12/2015–26/01/2016), the snow cover developed relatively fast and snow cover remained at more than 20 cm depth for most of the period. When T_{air} is dropped to more than −25 °C, the freeze and thaw periods became visible in the first 10 cm of the soil, except for the SFT section. At the beginning of second freezing period (11/02/2016–2/03/2016), snow cover was shallower (<20 cm depth) and relatively smaller drop of T_{air} (compared with the first freezing period) correlated with a deeper freezing effect in the soil profiles ($T_{soil} < 0$ °C at up to 40 cm depth in NFT). These observed T_{soil} trends are in agreement with observations made in previous studies (e.g., Sutinen et al, 2008; Zhao et al 2013).

However, it was interesting to see the differences in T_{soil} between the sections along the monitored transects. In general, T_{soil} observed within the north-facing slope (NFT, NFM and NFB), was lower than T_{soil} observed within the south-facing slope (SFT, SFM and SFB). The largest differences were visible in freeze–thaw periods observed during the second freezing period: in north-facing slope, $T_{soil} < 0$ °C was observed down to 40 cm depth (NFT) while in south-facing slope soil freezing was observed only down to 10 cm depth (SFM). The SFB sections appeared to be the warmest, with no soil freezing during that period. The observations also showed that north-facing sections warmed up slower than did south-facing sections during the snowmelt period at the end of the winter season: at the end of the monitoring period (from 20/03/2016), T_{soil} in south-facing slope was around 3 °C and in north-facing slope between 0.3 and 0.9 °C.

Vertical profiles of θ_{liquid} observed along the transect are presented in Fig. 5. At the beginning of the experiment (12/11/2015–11/12.2015) when the T_{air} was still oscillating around 0 °C and there was no snow cover, θ_{liquid} ranged between 0.26 and 0.36 $m^3.m^{-3}$ in all six profiles. The highest values of θ_{liquid} were observed in the bottom sections (SFB and NFB), and the lowest values in the top sections (SFT and NFT). During two freezing periods (25/12/2015 – 26/01/2016 and 11/02/2016–13/03/2016), θ_{liquid} decreased significantly, reaching 0.04 $m^3.m^{-3}$ in the near-surface soil layers (0–0.10 m) of the north-facing slope. This can be related to freezing of water in the larger pores and, consequently, reduced θ_{liquid} in favour of increased ice content (see also Fig. 6). The θ_{liquid} was relatively stable over the vertical profiles in time, during the two freezing periods, while more dynamic behaviour was observed during periods of thawing and snow melting (when T_{air} stayed above 0 °C; 27/01/2016 – 10/02/2016 and after 18/03/2016). The general spatial trends remained the same: lower values were observed in the top sections (SFT and NFT) and higher values were observed in the sections at the bottom of the slopes (SFB, NFB). This is a consequence of water drainage to the lower parts and concentration of flow at the bottom of the depression.

Differences were also observed in θ_{liquid} between the north-facing and south-facing slope. The observed periods with (partly) frozen soil water (low θ_{liquid}) were generally longer in the north-facing slope and soil water freezing reached deeper there (Figs. 4 and 5). When looking at the differences between the sections within the slopes, trends in the freezing depths are similar: the top sections (NFT and SFT) showed deeper soil freezing than sections at the bottom (NFB and SFB). Moreover, during

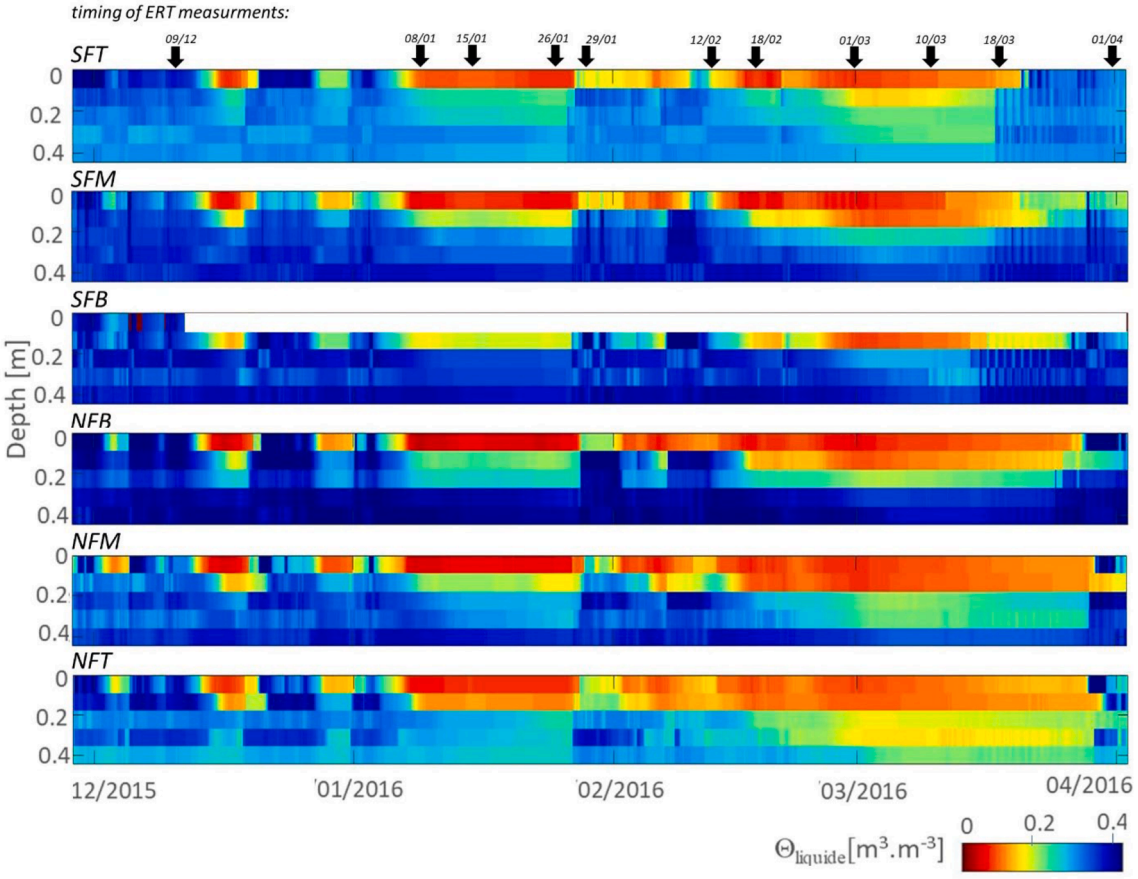

Fig. 5. Measured liquid water content (θ_{liquid}) in vertical soil profiles (0.05, 0.10, 0.20, 0.30, 0.40 m depth) at six locations along the experimental transect (SFT, SFM, SFB, NFB, NFM, NFT). The white area within the SFB section indicates periods with no measurements due to technical problems. The black arrows indicate the dates when ERT measurements were performed.

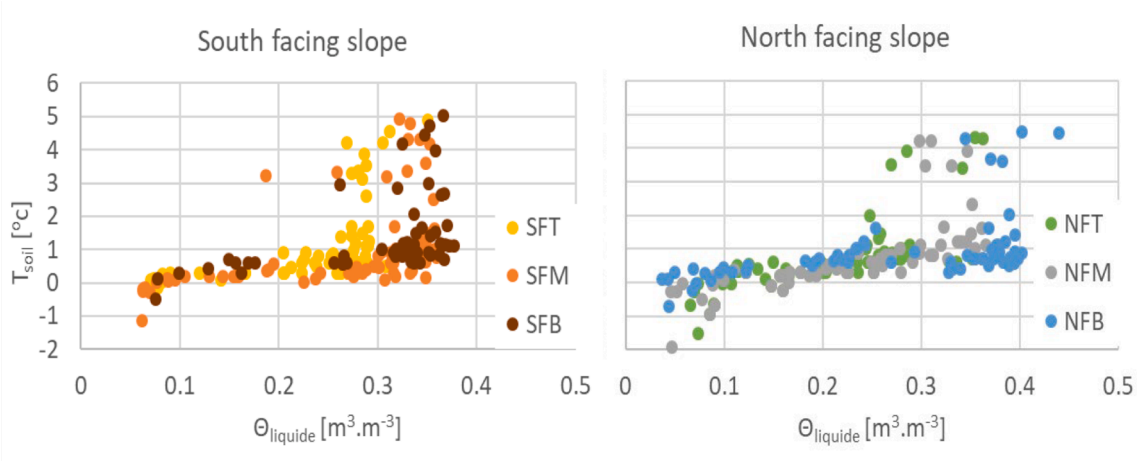

Fig. 6. Liquid water content (Θ_{liquid}) versus soil temperature (T_{soil}) measured within vertical soil profiles (0.05, 0.10, 0.20, 0.30, 0.40 m depth).

the snowmelt at the end of the winter period, it is clearly visible that snowmelt infiltration associated with thawing processes started sooner in south-facing slope than in north-facing slope. These temporal and spatial heterogeneities in θ_{liquid} patterns correlate with the trends observed in T_{soil} patterns (Fig. 4).

Fig. 6 shows the relationship between θ_{liquid} and T_{soil} measured within vertical soil profiles. For the soil temperatures between 2 °C and −1°C, the whole range of possible θ_{liquid} was measured (Fig. 6). In winter conditions, these indicate freezing processes whereby soil water starts to freeze and therefore liquid water content decreases in favour of increasing ice content (not measured).

4.2. ERT measurements

Fig. 7 shows the ERT inversion results (resistivity ®) of the time-lapse datasets collected during winter 2015/2016. In general, trends observed in *R* values followed the same trend as observed for θ_{liquid}. (Figs. 4 and 5). There was an increase in *R* within the top layer of the soil during the cold winter days (08/01, 15/01, 12/02, 01/03, 10/03) followed by a decrease in resistivity during warmer winter days (26/01, 29/01, 12/02, 14/02) and spring (14/03, 01/04). Spatially, the top sections (NFT and SFT) showed the highest variation in resistivity values, followed by the middle sections (NFM and SFM). In general, there was faster and more extensive resistivity increase on the north-facing slope compared to south-facing slope.

In addition, series of anomalies in the *R* values were observed in the top and middle section of the south- facing slope (SFT and SFM) at deeper soil layers (down to 2.0 m). This is elaborated further in Section 5.1.

5. Discussion

This paper presents a set of field-based measurement that provide a basis for analysing spatial heterogeneities in subsurface soil moisture and soil temperature associated with freezing, thawing and snowmelt infiltration, and its relation to local terrain heterogeneities. Furthermore, these data can be used to elaborate on the influence of local terrain heterogeneities (i.e., slope and aspect) on soil erosion processes.

5.1. Relationship between R and Θ_{liquid}

The electrical resistivity (*R*) is the result of the combination of soil texture, water content and salt concentration. In the case of time-lapse resistivity measurements, changes in water content and salt concentrations can be observed, while soil texture is constant. In our study, we would not expect any changes in salt concentration. Therefore, observed changes occurring in the experimental ERT transect can be related to changes in water/ice content in the soil.

The calculated *R* values were in range of 'typical resistivity values' reported in previous studies; for example, while unfrozen soils have typical resistivity values from a few to hundreds of ohm-metres, depending on pore water salinity, saturation, soil type and texture, typical resistivity values for frozen soils ranges from tens to hundreds of kilo-ohm-meters (French et al., 2006, Krautblatter and Hauck, 2007, Fortier et al., 2008, Dafflon et al., 2013).

In general, trends in calculated *R* values (Fig. 7) followed observed spatial variation in θ_{liquid} (Fig. 5).

Fig. 8 shows the correlation between θ_{liquid} and *R*, divided by the slope sections (NFT, NFM, NFB, SFB, SFM, SFT), with an additional distinction between freezing and thawing periods. Average θ_{liquid} from the day of the ERT measurement is collated with average *R* value representative for each FDR location.

While it is difficult to see correlation between *R* and Q_{liguid}, high R values occur at low θ_{liquid} while lower R values are mostly associated with higher θ_{liquid}. There are visible differences in behaviours/trends between the north-facing and south-facing slope as well as between sections within the slopes. In general, the ranges of both Q_{liguid} and *R* values observed for the north-facing slope was wider than that one observed for the south-facing sections. It is especially visible in case of top sections (*NFT* vs *SFT*).

These indicate that, for frozen conditions slope aspect and consequently exposition and (depth of) snow cover and may have additional influence on both *R* and Q_{liguid} spatial and temporal behaviour: e.g., differences in (depth of) snow cover between north-facing and south-facing slope observed during thawing period (Fig. 10).

5.2. ERT measurement: Data quality and error analysis

A series of anomalies were observed within the *R* values in the top and middle section of the south-facing slope (SFT and SFM), reaching deeper soil layers (down to 2.0 m), that cannot be explained by current θ_{liquid} and T_{soil} measures or by previous studies (e.g., soil heterogeneities). The quality of ERT data was assessed by looking at the percentage of outliers (measurements with an error between the normal and reciprocal higher than 10%) in each of the collected raw ERT data sets. 'Good quality data sets' are ones that have no or a limited number of outliers. This means that (nearly) 100% of raw data was used for inversion modelling, and consequently gave the most accurate estimates for 2D apparent resistivity mapping.

The quality of the collected raw ERT data shows significant differences between data sets from different time periods (Fig. 9). On the days when the quality of the dataset collected was lower (Fig. 9), more

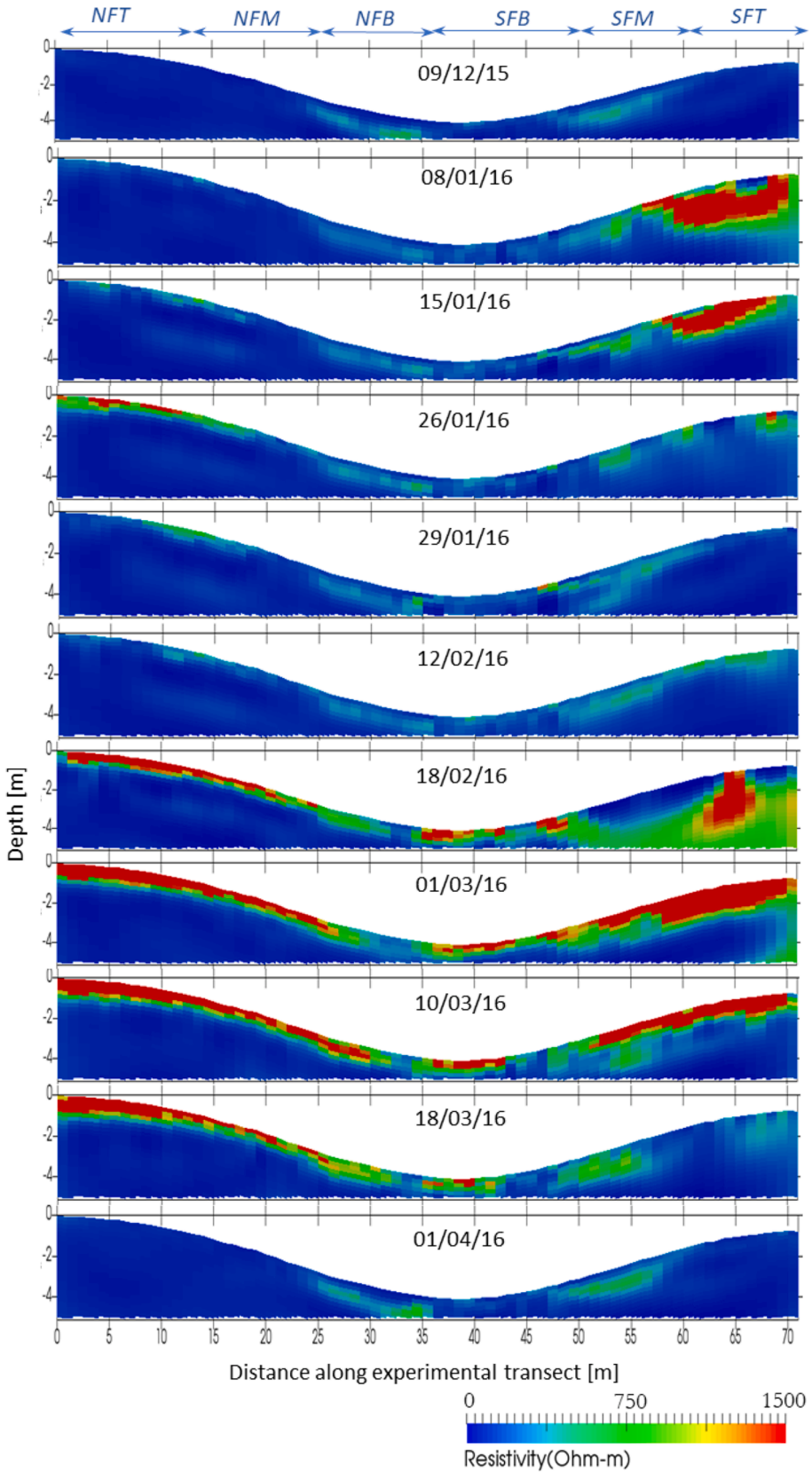

Fig. 7. Set of ERT inversion results. Each panel represent the measuring transect on the day the ERT measurement were performed. The sections (NFT, NFM, NFB, SFB, SFM, SFT) are delineated at the top of the figure.

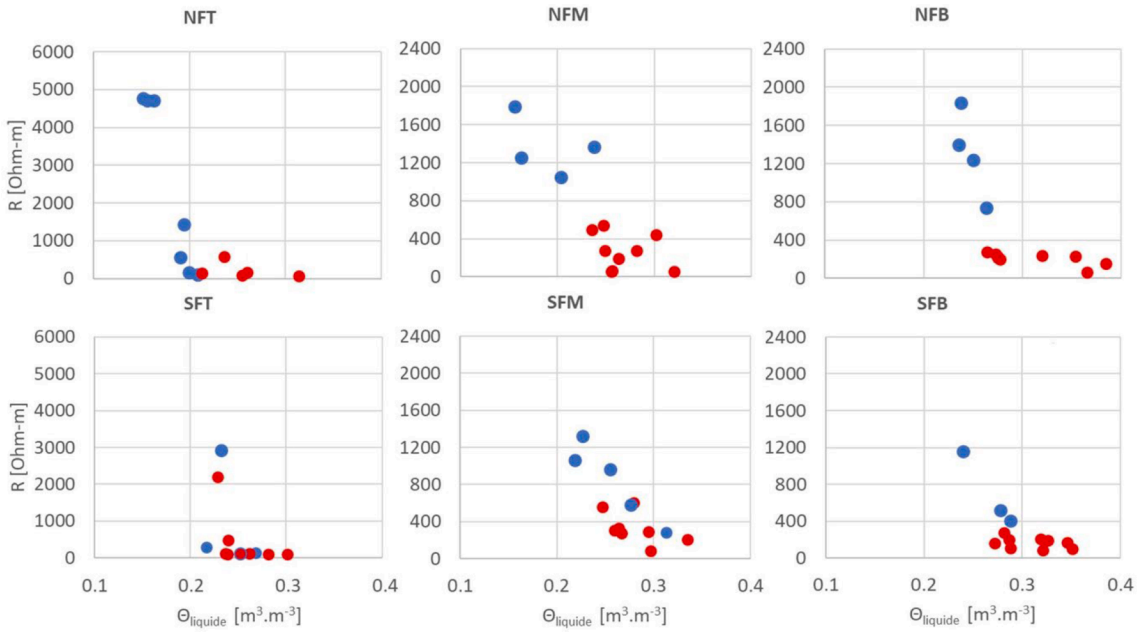

Fig. 8. The relationship between R and θ_{liquid} for all six sections along the ERT transect. Blue dots correspond to days when soil was (partly) frozen (T_{soil} was below 0.5–0.9 °C depending on the section; see Fig. 6) and red dots correspond to thawing periods (T_{soil} was above 0.5–0.9 °C depending on the section; see Fig. 6).

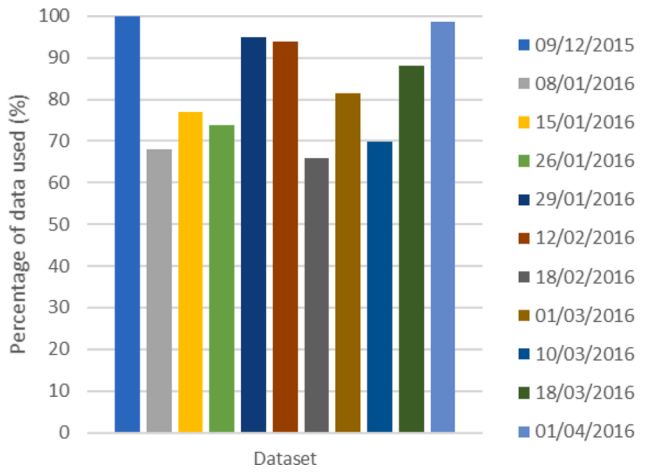

Fig. 9. The quality of each dataset, by the percentage of each dataset with errors between normal and reciprocal measurements <100%.

anomalies within calculated R values were observed (Fig. 7). In general, the dates on which lower quality ERT data were collected correspond with dates on which the T_{soil} was the lowest. Therefore, outlying values can be explained by potential problems with establishing good connection between electrodes and frozen soil. This should be considered in further analyses.

5.3. Potential influence of slope aspect on soil erosion

The simplistic scheme of initiating soil erosion (sheet erosion and gully erosion) starts with the impact of raindrops on bare soil to disperse soil aggregates. Then, when the rainfall intensity exceeds the infiltration capacity of the soil, water accumulates on the surface, and surface runoff is initiated. Depending on the erosive force and transport capacity of the waterflow, soil detachment and deposition will occur. While the most important factors of runoff generation and surface erosion processes are local weather conditions and soil management practices (e.g., snowmelt and precipitation timing and amount, tillage timings, etc), the results presented in this study allow to elaborate on potential influence of local terrain heterogeneities on soil erosion initiating processes. Observed patterns in soil temperature and liquid water content can affect soil infiltration capacity, runoff generation (e.g., Beven, 2000; Woods et al., 2001) and erosion patterns. Slope aspect (south-facing slope vs. north-facing slope) and location on the slope (top, middle, bottom) influence the soil temperature (Fig. 4) and liquid water content (Fig. 5) (Barneveld et al., 2019).

Previous research at the Gryteland catchment dedicated to catchment hydrology during winter and spring (Starkloff et al., 2017) shows that one of the important factors, determining the extent of runoff and erosion during the winter period is whether the soil is frozen or unfrozen at a particular moment of precipitation or/and snowmelt event. The monitoring data presented in this paper show that north-facing slope froze earlier and deeper than the south-facing slopes. The spring thawing period started significantly earlier on the south-facing slope and spread throughout the vertical soil profile. This pattern was observed in the Gryteland catchment before (Starkloff et al. 2017) as well as during ERT monitoring period (Fig. 10). As such, depending on the snowmelt and precipitation timing, it can have both positive (snowmelt infiltrates before spring rainfalls) and negative (culmination of snowmelt together with spring rainfalls) influence on runoff generation and surface erosion. Even if the surface soil layer is not frozen, the probability for existence of frozen layers of soil deeper in the profile is higher. This can significantly influence infiltration processes and accelerate initiation or/and increase amount of runoff. Consequently, north-facing slope could be more affected by surface erosion. This, in turn, is in agreement with what was observed in the field and modelled by Starkloff et al. (2018) in Gryteland catchment.

In terms of soil liquid water content trends, there is little difference between the bottom sections (NFB and SFB). They are generally the most wet sections and have similar timing of freezing/thawing periods. Their location at the bottom, and being the wettest part of the slope, also makes them prone to surface erosion. The runoff from the upper parts accumulates in the bottom sections of this depression. This is commonly observed in the Gryteland catchment as shown in Fig. 2 or in work of Starkloff et al. (2018). The wet soil, with its limited infiltration capacity and reduced shear strength, combined with concentrated runoff can easily be eroded (Starkloff et al., 2017)

Fig. 10. Gryteland catchment, photo taken on 18/03/2016, during the thawing period. A view of the depression, where the ERT transect was installed. (Photo: T. Starkloff).

In addition, freeze–thaw cycles can influence aggregate stability. Starting with the analysis of the freezing period, aggregate stability is inversely proportional to soil water content at the time of freezing (e.g., Perfect et al., 1990, Lehrsch, 1998). Since the bottom sections of both slopes are the wettest areas, this would suggest that they also have the lowest aggregate stability. Several studies have reported that the aggregate stability increases with the onset of the first one to three freeze–thaw cycles but decreased thereafter (Lehrsch, 1998; Angin et al., 2016). Additionally, Kværnø and Øygarden (2006) showed that, for Norwegian clay soils, aggregate stability decreases significantly with the increasing number of freeze–thaw cycles. In our case, freeze–thaw cycles are less visible on the north-facing slope compared with the south-facing slope (as a consequence of deeper and longer freezing of the north facing slope), suggesting potential differences in surface erosion patterns.

6. Conclusions

Seasonal monitoring of soil temperature and soil moisture gives an insight into temporal changes in the subsurface state during freeze–thaw cycles. Moreover, it shows that even small-scale terrain heterogeneities (local slope and aspect), influence the distribution of soil freezing horizontally and vertically. Observed temperature and soil moisture patterns are in agreement with previous research: north-facing slopes have longer freezing periods than south-facing slopes. Additionally, as shown in the presented study, soil freezing is deeper on north-facing slope than on south-facing slope.

Observed resistivity patterns with ERT correspond well to the measured soil moisture (θ_{liquid}) patterns. The differences between resistivity and θ_{liquid} observed in the six sections can be explained by changes in slope and aspect (south-facing vs north-facing slope). The first attempt to quantify the resistivity measured with ERT versus θ_{liquid} (Figs. 7 and 8) gives promising results. Even though not a fully independent measure, ERT is a very useful method to reveal the heterogeneity in θ_{liquid} along the transect and could therefore be used to interpolate between the point measurements and reduce overall uncertainty in spatial interpretation of the results. A combination is highly recommended.

The results indicate that spatial terrain heterogeneities may be important when studying soil erosion processes, water flow and nutrient leaching in Nordic conditions. They show that initiation and development of runoff related processes and consequently soil erosion in regions with freeze–thaw cycles, may differ significantly depending on local terrain characteristic such as north-facing slope versus south-facing slope.

Knowing that local terrain heterogeneities can influence soil erosion processes in winter conditions, the findings presented in this paper can provide an important insight for interpreting soil erosion modelling results, and potential differences between modelled and monitored values, at field and catchment scale. Moreover, it indicates the need for spatially distributed monitoring of soil parameters and snow conditions at field and catchment scale and for more focus on slope aspect when modelling (sub-)soil conditions during freeze–thaw cycles and snowmelt infiltration.

Declaration of Competing Interest

The authors declare that they have no known competing financial interests or personal relationships that could have appeared to influence the work reported in this paper.

References

Alamry, A.S., van der Meijde, M., Noomen, M., Addink, E.A., van Benthem, R., de Jong, S.M., 2017. Spatial and temporal monitoring of soil moisture using surface electrical resistivity tomography in Mediterranean soils. Catena 157, 388–396.

Al-Houri, Z.M., Barber, M.E., Yonge, D.R., Ullman, J.L., Beutel, M.W., 2009. Impact of frozen soils on the performance of infiltration treatment facilities. Cold Reg. Sci. Technol. 59, 51–57.

Angin, I., Sari, S., Aksakal, E.L., 2016. Effects of diatomite (DE) application on physical properties of soils subjected to freeze-thaw cycles. Soil Tillage Res. 160, 34–41.

Ban, Y., Lei, T., Liu, Z., Chen, C., 2016. Comparison of rill flow velocity over frozen and thawed slopes with electrolyte tracer method. J. Hydrol. 534, 630–637.

Barneveld, R.J., Zee, S.E.A.T.M., Stolte, J., 2019. Quantifying the dynamics of microtopography during a snowmelt event. Earth Surf. Proc. Land. 44 (13), 2544–2556. https://doi.org/10.1002/esp.4678.

Beven, K.J., 2000. Rainfall Runoff Modelling: The Primer. John Wiley, Chichester.

Binley, A., 2013. R2 manual. Issue Univerity of Lancaster. Vol v2.7a.

Binley, A., 2015. Tools and Techniques: DC Electrical Methods. In: Schubert, G. (Ed.), Treatise on Geophysics, second ed., vol. 11. Elsevier, pp. 233–259. https://doi.org/10.1016/B978-0-444-53802-4.00192-5.
Binley, A., Kemna, A., 2005. DC Resistivity and Induced Polarization Methods. In: Rubin, Y., Hubbard, S.S. (Eds.), Water Science and Technology LibraryHydrogeophysics. Springer Netherlands, Dordrecht, pp. 129–156.
Boardman, J., Shepheard, M.L., Walker, E., Foster, I.D.L., 2009. Soil erosion and risk-assessment for on- and off-farm impacts: a test case using the Midhurst area, West Sussex, UK. J. Environ. Manage. 90 (8), 2578–2588.
Cassiani, G., Bruno, V., Villa, A., Fusi, N., Binley, A.M., 2006. A saline tracer test monitored via time-lapse surface electrical resistivity tom-ography. J. Appl. Geophys. 59, 244–259.
Cheviron, B., Guérin, R., Tabbagh, A., Bendjoudi, H., 2005. Determining long-term effective groundwater recharge by analyzing vertical soil temperature profiles at meteorological stations. Water Resour. Res. 41 (9) https://doi.org/10.1029/2005WR004174.
Constantz, J., Tyler, S.W., Kwicklis, E., 2003. Temperature-Profile Methods for Estimating Percolation Rates in Arid Environments. Vadose Zone J. 2 (1), 12–24.
Dafflon, B., Wu, Y., Hubbard, S.S., Birkholzer, J.T., Daley, T.M., Pugh, J.D., Peterson, J. E., Trautz, R.C., 2013. Monitoring CO2 intrusion and associated geochemical transformations in a shallow groundwater system using complex electrical methods. Environ. Sci. Technol. 47 (1), 314–321.
Deelstra, J., Kværnø, S.H., Granlund, K., Sileika, A.S., Gaigalis, K., Kyllmar, K., Vagstad, N., 2009. Runoff and nutrient losses during winter periods in cold climates – requirements to nutrient simulation models. J. Environ. Monit. 11 (3), 602. https://doi.org/10.1039/b900769p.
Deelstra, J., Øygarden, L., Blankenberg, A.B., Eggestad, H.O., 2011. Climate change and runoff form agricultural catchment in Norway. Clim. Change Strat. Manage. 3, 345–360.
Depountis, N., Harris, C., Davies, M.R.C., 2001. An assessment of miniaturized electrical imaging equipment to monitor pollution plume evolution in scaled centrifuge modelling. Eng. Geol. 60, 83–94.
Fortier, R., LeBlanc, A.-M., Allard, M., Buteau, S., Calmels, F., 2008. Internal structure and conditions of permafrost mounds at Umiujaq in Nunavik, Canada, inferred from field investigation and electrical resistivity tomography. Can. J. Earth Sci. 45, 367–387.
French, H., Binley, A., 2004. Snowmelt Infiltration: Monitoring Temporal and Spatial Variability using Time-Lapse Electrical resistivity. J. Hydrol. 297 (1–4), 174–186.
French, H.K, Binley, A., Kharkhordin, I., Kulessa, B., Krylov, S., 2006. Cold regions hydrogeophysics: physical characterisation and monitoringVereecken, H., Binley, A., Cassiani, G., Revil, A., Titov, K. (Eds.), In: Applied Hydrogeophysics. NATO Science Series, 71. Springer, Dordrecht, pp. 195–232.
French, H.K., Hardbattle, C., Binley, A., Winship, P., Jakobsen, L., 2002. Monitoring snowmelt induced unsaturated flow and transport using electrical resisitivity tomography. J. Hydrol. 267, 273–284.
He, H., Dyck, M.F., Si, B.C., Zhang, T., Lv, J., Wang, J., 2015. Soil freezing – thawing characteristics and snowmelt infiltration in Cryalfs of Alberta, Canada. Geodermal Reg. 5, 198–208.
Holten, R., Bøe, F.N., Almvik, M., Katuwal, S., Stenrød, M., Larsbo, M., Jarvis, N., Eklo, O. M., 2018. The effect of freezing and thawing on water flow and MCPA leaching in partially frozen soil. J. Contam. Hydrol. 219, 72–85.
Hubbard, S., Rubin, Y., 2000. Hydrogeological parameter estimation using geological data: A review of selected techniques. J. Contam. Hydrol. 45, 3–34.
Ireson, A., Kamp, G., Ferguson, G., Nachshon, U., Wheater, H.S., 2013. Hydrogeological processes in seasonally frozen northern latitudes: Understanding, gaps and challenges. Hydrogeol. J. 21, 53–66.
Iwata, Y., Nemoto, M., Hasegawa, S., Yanai, Y., Kuwao, K., Hirota, T., 2011. Influence of rain, air temperature, and snow cover on subsequent spring-snowmelt infiltration into thin frozen soil layer in northern Japan. J. Hydrol. 401, 165–176.
Jayawickreme, D.H., van Dam, R.L., Hyndman, D.W., 2008. Subsurface Imaging of Vegetation, Climate, and Root-Zone Moisture Interactions. Geophys. Res. Lett. 35, L18404. https://doi.org/10.1029/2008GL034690.
Kemna, A., Binley, A., Day-Lewis, F., Englert, A., Tezkan, B., Vanderborght, J., Vereecken, H., Winship, P., 2006. Appl. Hydrogeophys. 71, 117–159.
Krautblatter, M., Hauck, C., 2007. Electrical resistivity tomography monitoring of permafrost in solid rock walls. J. Geophys. Res. Earth Surf. 112, F02S20.
Kværnø, S.H., Øygarden, L., 2006. The influence of freeze-thaw cycles and soil moisture on aggregate stability of three soils in Norway. Catena 67 (3), 175–182.
Laker, M.C., 2004. Advances in soil erosion, soil conservation, land suitability evaluation and land use planning research in South Africa, 1978-2003. S. Afr. 1. Plant Soil 21 (5), 345.
Lehrsch, G.A., 1998. Freeze–thaw cycles increase near-surface aggregate stability. Soil Sci. 163 (1998), 63–70.
Loke, M.H., 2000. Topographic modelling in resistivity imaging inversion. In: 62nd EAGE Conference& Technical Exhibition Extended Abstracts, D-2.
Lundekvam, H.E., Romstad, E., Øygarden, L., 2003. Agricultural policies in Norway and effects on soil erosion. Environ. Sci. Policy 6, 57–67.
Lundekvam, H., Skøien, S., 1998. Soil erosion in Norway. An overview of measurements from soil loss plots. Soil Use Manage. 14, 84–89.
Michot, D., Benderitter, Y., Dorigny, A., Nicoullaud, B., King, D., Tabbagh, A., 2003. Spatial and temporal monitoring of soil water content with an irrigated corn crop cover using surface electrical resistivity tomography. Water Resour. Res. 39 (5), 1138.
Nijland, W., van der Meijde, M., Addink, E.A., de Jong, S.M., 2010. Detection of soil moisture and vegetation water abstraction in a Mediterranean natural area using electrical resistivity tomography. Catena 81 (3), 209–216.
Ollesch, G., Kistner, I., Meissner, R., Lindenschmidt, K.-E., 2006. Modelling of snowmelt erosion and sediment yield in a small low-mountain catchment in Germany. Catena 68 (2-3), 161–176.
Øygarden, L., 2003. Rill and gully development during an extreme winter runoff event in Norway. Catena 50 (2–4), 217–242.
Perfect, E., Loon, W.K.P.V., Kay, B.D., Groenevelt, P.H., 1990. Influence of ice segregation and solutes on soil structural stability. Can. J. Soil Sci. 70 (4), 571–581.
Scherler, M., Hauck, C., Hoelzle, M., Stähli, M., Völksch, I., 2010. Meltwater infiltration into the frozen active layer at an alpine permafrost site. Permafrost Periglac. Process. 21 (4), 325–334.
Shanley, J.B., Chalmers, A., 1999. The effect of frozen soil on snowmelt runoff at Sleepers River, Vermont. Hydrol. Process. 13 (12–13), 1843–1857.
Solbakken, E., 2015. Kartlegging av Gryteland delnedbørfelt. Skog og landskap Report, Ås, Norway (in Norwegian).
Starkloff, T., Hessel, R., Stolte, J., Ritsema, C., 2017. Catchment hydrology during winter and the link to soil erosion: A case study in Norway. Hydrology 4, 15. https://doi.org/10.3390/hydrology4010015.
Starkloff, T., Stolte, J., Hessel, R., Ritsema, C., Jetten, V., 2018. Integrated, spatial distributed modelling of surface runoff and soil erosion during winter and spring. CATENA 166, 147–157.
Sutinen, R., Hänninen, P., Venäläinen, A., 2008. Effect of mild winter events on soil water content beneth snowpack. Cold Reg. Sci. Technol. 51, 56–67.
Tabbagh, A., Bendjoudi, H., Benderitter, Y., 1999. Determination of Recharge in Unsaturated Soils Using Temperature Monitoring. Water Resour. Res. 35 (8), 2439–2446.
Thue-Hansen, V., Grimenes, A.A., 2014. Meteorologiske Data for Ås. Norges Miljø og Biovitenskaplige Universitet, Ås, Norway, pp. 2013–2014.
Vereecken, H., Binley, A., Cassiani, G., Revil, A., Titov, K. (Eds.), 2006. NATO Science SeriesApplied Hydrogeophysics. Springer Netherlands, Dordrecht.
Watanabe, K., Kito, T., Dun, S., Wu, J.Q., Greer, R.C., Flury, M., 2013. Water Infiltration into a Frozen Soil with Simultaneous Melting of the Frozen Layer. Vadose Zone J. 12 (1) https://doi.org/10.2136/vzj2011.0188.
Weigert, A., Schmidt, J., 2005. Water transport under winter conditions. Catena 64 (2–3), 193–208.
Woods, R.A., Grayson, R.B., Western, A.W., Duncan, M.J., Wilson, D.J., Young, R.I., Ibbitt, R.P., Henderson, R.D., McMahon, T.A., 2001. Experimental Design and Initial Results from the Rainfall-Runoff Processes Chapter 2: 19 Mahurangi River Variability Experiment: Marvex. In Observations and Modelling of Land Surface Hydrological Processes (Edited by V).
Yakutina, O.P., Nechaeva, T.V., Smirnova, N.V., 2015. Consequences of snowmelt erosion: Soil fertility, productivity and quality of wheat on Greyzemic Phaeozem in the south of West Siberia. Agric. Ecosyst. Environ. 200, 88–93.
Zhao, Y., Huang, M.B., Horton, R., Liu, F., Peth, S., Horn, R., 2013. Influence of winter grazing on water and heat flow in seasonal frozen soil of Inner Mongolia. Vadose Zone J. 12 vzj2012.0059.